1 Theory

1.1 Three-band tight-binding model

In the model introduced by Liu *et al.*, only the orbitals of the M atom are included. We denote the wave functions of the three orbitals of the M atom as

$$|\phi_1\rangle = |d_{z^2}\rangle\,, \quad |\phi_2\rangle = \left|d_{xy}\right\rangle\,, \quad |\phi_3\rangle = \left|d_{x^2-y^2}\right\rangle. \tag{1}$$

The Bloch wavefunction in this model has the form

$$\psi_{\mathbf{k}}^{\lambda}(\mathbf{r}) = \sum_{j=1}^{3} C_j^{\lambda}(\mathbf{k}) \sum_{\mathbf{R}} e^{i\mathbf{k}\cdot\mathbf{R}} \phi_j(\mathbf{r}-\mathbf{R}). \tag{2}$$

The coefficents $C_j^{\lambda}(\mathbf{k})$ are the solutions of the eigenvalue equation

$$\sum_{jj'}^{3} \left[H_{jj'}^{\mathrm{TB}}(\mathbf{k}) - \varepsilon_{\lambda}(\mathbf{k}) S_{jj'}(\mathbf{k})\right] C_j^{\lambda}(\mathbf{k}) = 0, \tag{3}$$

where

$$H_{jj'}^{\mathrm{TB}}(\mathbf{k}) = \sum_{\mathbf{R}} e^{i\mathbf{k}\cdot\mathbf{R}} \left\langle \phi_j(\mathbf{r})\right| H_{1\mathrm{e}} \left|\phi_{j'}(\mathbf{r}-\mathbf{R})\right\rangle, \tag{4}$$

and

$$S_{jj'}(\mathbf{k}) = \sum_{\mathbf{R}} \left\langle \phi_j(\mathbf{r}) \middle| \phi_{j'}(\mathbf{r}-\mathbf{R})\right\rangle \approx \delta_{jj'}. \tag{5}$$

In the case $B \neq 0$, the new lattice vector now is $\mathbf{R} = k\mathbf{a}_1 + l2q\mathbf{a}_2$, where $k, l \in \mathbb{Z}$. The wavefunction has an additional phase factor

$$\psi_{\mathbf{k}}^{\lambda}(\mathbf{r}) = \sum_{j=1}^{3} C_j^{\lambda} \sum_{\mathbf{R}} e^{i\mathbf{k}\cdot\mathbf{R}} e^{i\theta_{\mathbf{R}}(\mathbf{r})} \phi_j(\mathbf{r}-\mathbf{R}), \tag{6}$$

and choose $\theta = -\frac{e}{\hbar}\int_{\mathbf{r}}^{\mathbf{R}} \mathbf{A}(\mathbf{r}')\cdot d\mathbf{r}'$ as Peierls phase factor, the Hamiltonian now is

$$H_{jj'} = \sum_{\mathbf{R}} e^{i\mathbf{k}\cdot\mathbf{R}} e^{\frac{ie}{\hbar}\int_0^{\mathbf{R}} \mathbf{A}(\mathbf{r})\cdot d\mathbf{r}} E_{jj'}(\mathbf{R}), \tag{7}$$

where

$$E_{jj'} = \left\langle \phi_j(\mathbf{r})\right| H_{1e} \left|\phi_{j'}(\mathbf{r}-\mathbf{R})\right\rangle. \tag{8}$$

Using a uniform magnetic field $\mathbf{B} = (0, 0, B)$ and Landau gauge $\mathbf{A} = (By, 0, 0)$. The

Peierls hopping phase is given

$$\begin{aligned}\frac{ie}{\hbar}\int_{\mathbf{0}}^{\mathbf{R}}\mathbf{A}(\mathbf{r})\cdot d\mathbf{r} &= \frac{ie}{\hbar}\int_{\mathbf{0}}^{\mathbf{R}} By dx \\ &= \frac{ieB}{\hbar}\int_0^1 y(\tau)x'(\tau)d\tau,\end{aligned} \tag{9}$$

suppose that the atom M is located at lattice vector $\mathbf{R}_{m,n}$, the Peierls phase can be written as

$$\theta_{m,n}^{m',n'} = \begin{cases} 0 & m' = m \pm 2, n' = n, \\ 0 & m' = m \pm 4, n' = n, \\ \pm\frac{e}{\hbar}\frac{Ba^2\sqrt{3}}{2}m & m' = m, n' = n \pm 2, \\ \pm\frac{e}{\hbar}\frac{Ba^2\sqrt{3}}{4}\left(m \mp \frac{1}{2}\right) & m' = m \mp 1, n' = n \pm 1, \\ \pm\frac{e}{\hbar}\frac{Ba^2\sqrt{3}}{2}(m \mp 1) & m' = m \mp 2, n' = n \pm 2, \\ \pm\frac{e}{\hbar}\frac{Ba^2\sqrt{3}}{4}\left(m \mp \frac{3}{2}\right) & m' = m \mp 3, n' = n \pm 1. \end{cases} \tag{10}$$

We obtain the Hamiltonian in magnetic field

$$\begin{aligned} H_{jj'}^{\mathrm{TB}}(\mathbf{k}) &= E_{jj'}(\mathbf{0}) + e^{i\mathbf{k}\cdot\mathbf{R}_1}E_{jj'}(\mathbf{R}_1) + e^{-i\pi(m+1/2)\frac{\Phi}{\Phi_0}}e^{i\mathbf{k}\cdot\mathbf{R}_2}E_{jj'}(\mathbf{R}_2) \\ &+ e^{-i\pi(m-1/2)\frac{\Phi}{\Phi_0}}e^{i\mathbf{k}\cdot\mathbf{R}_3}E_{jj'}(\mathbf{R}_3) + e^{i\mathbf{k}\cdot\mathbf{R}_4}E_{jj'}(\mathbf{R}_4) \\ &+ e^{i\pi(m-1/2)\frac{\Phi}{\Phi_0}}e^{i\mathbf{k}\cdot\mathbf{R}_5}E_{jj'}(\mathbf{R}_5) + e^{i\pi(m+1/2)\frac{\Phi}{\Phi_0}}e^{i\mathbf{k}\cdot\mathbf{R}_6}E_{jj'}(\mathbf{R}_6) \\ &+ e^{-i\pi(m+3/2)\frac{\Phi}{\Phi_0}}e^{i\mathbf{k}\cdot\mathbf{R}_7}E_{jj'}(\mathbf{R}_7) + e^{-2i\pi m\frac{\Phi}{\Phi_0}}e^{i\mathbf{k}\cdot\mathbf{R}_8}E_{jj'}(\mathbf{R}_8) \\ &+ e^{-i\pi(m-3/2)\frac{\Phi}{\Phi_0}}e^{i\mathbf{k}\cdot\mathbf{R}_9}E_{jj'}(\mathbf{R}_9) + e^{i\pi(m-3/2)\frac{\Phi}{\Phi_0}}e^{i\mathbf{k}\cdot\mathbf{R}_{10}}E_{jj'}(\mathbf{R}_{10}) \\ &+ e^{2i\pi m\frac{\Phi}{\Phi_0}}e^{i\mathbf{k}\cdot\mathbf{R}_{11}}E_{jj'}(\mathbf{R}_{11}) + e^{i\pi(m+3/2)\frac{\Phi}{\Phi_0}}e^{i\mathbf{k}\cdot\mathbf{R}_{12}}E_{jj'}(\mathbf{R}_{12}) \\ &+ e^{i\mathbf{k}\cdot\mathbf{R}_{13}}E_{jj'}(\mathbf{R}_{13}) + e^{-2i\pi(m+1)\frac{\Phi}{\Phi_0}}e^{i\mathbf{k}\cdot\mathbf{R}_{14}}E_{jj'}(\mathbf{R}_{14}) \\ &+ e^{-2i\pi(m-1)\frac{\Phi}{\Phi_0}}e^{i\mathbf{k}\cdot\mathbf{R}_{15}}E_{jj'}(\mathbf{R}_{15}) + e^{i\mathbf{k}\cdot\mathbf{R}_{16}}E_{jj'}(\mathbf{R}_{16}) \\ &+ e^{2i\pi(m-1)\frac{\Phi}{\Phi_0}}e^{i\mathbf{k}\cdot\mathbf{R}_{17}}E_{jj'}(\mathbf{R}_{17}) + e^{2i\pi(m+1)\frac{\Phi}{\Phi_0}}e^{i\mathbf{k}\cdot\mathbf{R}_{18}}E_{jj'}(\mathbf{R}_{18}), \end{aligned} \tag{11}$$

where $\Phi_0 = \frac{h}{e}$ and $\Phi = \frac{\sqrt{3}}{2}Ba^2$. Since the Peierls phase depends on the the atomic position specified by the site indices m, n, the Hamiltonian is no longer invariant under translation of a primitive vector. For the case $\frac{\Phi}{\Phi_0} = \frac{p}{q}$, with $p, q \in \mathbb{Z}$, it is possible to restore the translational invariance if we expand the unit cell so that it includes $2q$ M atoms. We, then, define a new basis set of $6q$ atomic orbitals $\left\{\phi_j(\mathbf{r} - \mathbf{R}_{m,n})\right\}$. The wave function can be expressed as the coefficients of C_{ji}^{λ} in the tight-binding wave function

$$\psi_{\mathbf{k}}^{\lambda}(\mathbf{r}) = \sum_{j}^{3}\sum_{i}^{2q} C_{ji}^{\lambda}(\mathbf{k}) \sum_{\mathbf{R}} e^{\frac{ie}{\hbar}\int_0^{\mathbf{R}+\mathbf{R}_i}\mathbf{A}(\mathbf{r})\cdot d\mathbf{r}} e^{i\mathbf{k}\cdot(\mathbf{R}+\mathbf{R}_i)}\phi_j(\mathbf{r}-\mathbf{R}-\mathbf{R}_i). \tag{12}$$

where $j = 1, 2, 3$ and i labels the atom $\mathbf{R}^{(i)}$ in the magnetic unit cell, with $i = 1, \ldots, 2q$. In this basis, the TB Hamiltonian has an additional Peierls phase

$$H_{jij'i'} = \sum_{\mathbf{R}} e^{i\mathbf{k}\cdot(\mathbf{R}-\mathbf{R}_i+\mathbf{R}_{i'})} e^{\frac{ie}{\hbar}\int_{\mathbf{R}_i}^{\mathbf{R}+\mathbf{R}_{i'}}\mathbf{A}(\mathbf{r})\cdot d\mathbf{r}} \left\langle \phi_j(\mathbf{r}-\mathbf{R}_i) \right| H_{1e} \left| \phi_{j'}(\mathbf{r}-\mathbf{R}-\mathbf{R}_{i'}) \right\rangle, \tag{13}$$

The sum over $\mathbf{R}$ include up to third-nearest-neighbor hoppings. It is remarkbly to note that the lattice vectors satisfying the condition $|\mathbf{R}| \le 2a$ are $\mathbf{R} = \mathbf{0}, \pm\mathbf{a}_1, \pm 2\mathbf{a}_1$, we obtain the Hamiltonian

$$\begin{aligned}
H^{\text{eff}}_{jnj'n'}(\mathbf{k}) &= E_{jj'}(\mathbf{0})\delta_{n,n'} + e^{i\mathbf{k}\cdot\mathbf{R}_1}E_{jj'}(\mathbf{R}_1)\delta_{n,n'} + e^{i\mathbf{k}\cdot\mathbf{R}_4}E_{jj'}(\mathbf{R}_4)\delta_{n,n'} \\
&+ e^{-i\pi(m+1/2)\frac{\Phi}{\Phi_0}} e^{i\mathbf{k}\cdot\mathbf{R}_2}E_{jj'}(\mathbf{R}_2)\delta_{n-1,n'} + e^{-i\pi(m-1/2)\frac{\Phi}{\Phi_0}} e^{i\mathbf{k}\cdot\mathbf{R}_3}E_{jj'}(\mathbf{R}_3)\delta_{n-1,n'} \\
&+ e^{i\pi(m-1/2)\frac{\Phi}{\Phi_0}} e^{i\mathbf{k}\cdot\mathbf{R}_5}E_{jj'}(\mathbf{R}_5)\delta_{n+1,n'} + e^{i\pi(m+1/2)\frac{\Phi}{\Phi_0}} e^{i\mathbf{k}\cdot\mathbf{R}_6}E_{jj'}(\mathbf{R}_6)\delta_{n+1,n'} \\
&+ e^{-i\pi(m+3/2)\frac{\Phi}{\Phi_0}} e^{i\mathbf{k}\cdot\mathbf{R}_7}E_{jj'}(\mathbf{R}_7)\delta_{n-1,n'} + e^{-2i\pi m\frac{\Phi}{\Phi_0}} e^{i\mathbf{k}\cdot\mathbf{R}_8}E_{jj'}(\mathbf{R}_8)\delta_{n-2,n'} \\
&+ e^{-i\pi(m-3/2)\frac{\Phi}{\Phi_0}} e^{i\mathbf{k}\cdot\mathbf{R}_9}E_{jj'}(\mathbf{R}_9)\delta_{n-1,n'} + e^{i\pi(m-3/2)\frac{\Phi}{\Phi_0}} e^{i\mathbf{k}\cdot\mathbf{R}_{10}}E_{jj'}(\mathbf{R}_{10})\delta_{n+1,n'} \\
&+ e^{2i\pi m\frac{\Phi}{\Phi_0}} e^{i\mathbf{k}\cdot\mathbf{R}_{11}}E_{jj'}(\mathbf{R}_{11})\delta_{n+2,n'} + e^{i\pi(m+3/2)\frac{\Phi}{\Phi_0}} e^{i\mathbf{k}\cdot\mathbf{R}_{12}}E_{jj'}(\mathbf{R}_{12})\delta_{n+1,n'} \\
&+ e^{i\mathbf{k}\cdot\mathbf{R}_{13}}E_{jj'}(\mathbf{R}_{13})\delta_{n,n'} + e^{-2i\pi(m+1)\frac{\Phi}{\Phi_0}} e^{i\mathbf{k}\cdot\mathbf{R}_{14}}E_{jj'}(\mathbf{R}_{14})\delta_{n-2,n'} \\
&+ e^{-2i\pi(m-1)\frac{\Phi}{\Phi_0}} e^{i\mathbf{k}\cdot\mathbf{R}_{15}}E_{jj'}(\mathbf{R}_{15})\delta_{n-2,n'} + e^{i\mathbf{k}\cdot\mathbf{R}_{16}}E_{jj'}(\mathbf{R}_{16})\delta_{n,n'} \\
&+ e^{2i\pi(m-1)\frac{\Phi}{\Phi_0}} e^{i\mathbf{k}\cdot\mathbf{R}_{17}}E_{jj'}(\mathbf{R}_{17})\delta_{n+2,n'} + e^{2i\pi(m+1)\frac{\Phi}{\Phi_0}} e^{i\mathbf{k}\cdot\mathbf{R}_{18}}E_{jj'}(\mathbf{R}_{18})\delta_{n+2,n'}.
\end{aligned} \tag{14}$$

where $\Phi_0 = \frac{h}{e}$, $\Phi = \frac{\sqrt{3}}{2}Ba^2$ and $E(\mathbf{R})$ are obtained from Liu *et al.*

1.2 The cyclotron theory

The cyclotron frequency can be obtained from the energy difference between two Landau levels

$$\hbar\omega_c = E_{n+1} - E_n, \tag{15}$$

which gives

$$\omega_c = \frac{E_{n+1} - E_n}{\hbar}. \tag{16}$$

On the other hand, the cyclotron frequency is also defined as

$$\omega_c = \frac{eB}{m^*}. \tag{17}$$

Combining the two expressions, the effective mas can be written as

$$m^* = \frac{eB}{\omega_c} = \frac{eB}{\frac{E_{n+1}-E_n}{\hbar}} = \frac{eB\hbar}{E_{n+1} - E_n}, \tag{18}$$

and

$$\omega_c = \frac{E_{n+1} - E_n}{\hbar}. \tag{19}$$

The radius of cyclotron orbit can be written as

$$r_c = \frac{v_\perp}{\omega_c} = \frac{v_\perp \hbar}{E_{n+1} - E_n} = \frac{v_\perp m^*}{eB}, \tag{20}$$

where $v_\perp$ is choosen to be equal to 3×10^7 m/s.

2 Methods

When a magnetic field is applied to the crystal lattice, the magnetic unit cell is enlarged q times for square lattice ($2q$ times for hexagonal lattice). As a consequence, the magnetic Brillouin zone smaller $2q$ times than the orginal Brillouin zone.

In addition, the three bases $d_{z^2}, d_{xy}, d_{x^2-y^2}$, which were introduced by Liu *et al.*, cannot clearly distinguish the K and K' points in the valence and conduction bands for two reasons. First, the squared amplitudes $|\psi|^2$ are identical. Second, in the magnetic Brillouin zone, the K and K' valleys cannot be intuitively distinguished by the dispersion relation $E(\mathbf{k})$; instead, one needs to examine the properties of the wave functions. Specifically, the electron wave function at the K valley in conduction band is mainly contributed by d_{z^2}, while at the valence band it is $d_{xy} + d_{x^2-y^2}$. Furthemore, we can distingushed K and K' valleys at the valence by using bases

$$\left|\psi_v^K\right\rangle = \frac{1}{\sqrt{2}} \left(\left|d_{x^2-y^2}\right\rangle + i \left|d_{xy}\right\rangle \right), \tag{21}$$

$$\left|\psi_v^{K'}\right\rangle = \frac{1}{\sqrt{2}} \left(\left|d_{x^2-y^2}\right\rangle - i \left|d_{xy}\right\rangle \right). \tag{22}$$

Therefore, it is necessary to adopt another basis set. We now consider a new basis consisting of the three eigenfunctions of the angular momentum operators L^2 and L_z, corresponding to $l = 2$ and $m = 0, \pm 2$.

$$\left|\tilde{\phi}_1\right\rangle = \left|d_{m=0}\right\rangle, \quad \left|\tilde{\phi}_2\right\rangle = \left|d_{m=+2}\right\rangle, \quad \left|\tilde{\phi}_3\right\rangle = \left|d_{m=-2}\right\rangle. \tag{23}$$

The new basis can be obtained from the old one by the transformation

$$\left|\tilde{\phi}_j\right\rangle = \sum_{j'} W_{j'j} \left|\phi_{j'}\right\rangle, \tag{24}$$

where

$$W = \begin{pmatrix} 1 & 0 & 0 \\ 0 & \frac{i}{\sqrt{2}} & -\frac{i}{\sqrt{2}} \\ 0 & \frac{1}{\sqrt{2}} & \frac{1}{\sqrt{2}} \end{pmatrix}. \tag{25}$$

In particular,

$$\left|\tilde{\phi}_1\right\rangle = \left|\phi_1\right\rangle, \tag{26}$$

$$\left|\tilde{\phi}_2\right\rangle = \frac{i}{\sqrt{2}} \left|\phi_2\right\rangle + \frac{1}{\sqrt{2}} \left|\phi_3\right\rangle, \tag{27}$$

$$\left|\tilde{\phi}_3\right\rangle = -\frac{i}{\sqrt{2}} \left|\phi_2\right\rangle + \frac{1}{\sqrt{2}} \left|\phi_3\right\rangle. \tag{28}$$

The TB Hamiltonian in new basis reads

$$\tilde{H}^{\mathrm{TB}}(\mathbf{k}) = W^\dagger H^{\mathrm{TB}}(\mathbf{k}) W, \tag{29}$$

where $H^{\mathrm{TB}} = H^{\mathrm{NN}}$ or H^{TNN}.

To distinguish the states that originate from the original Brillouin zone, we follow the convention of Ho *et al.* [1]. Each Landau level is then labeled as $\left|j, n\right\rangle_\tau$, where j, n, and τ denote the orbital, Landau, and valley indices, respectively.

When diagonalizing the Hamiltonian in Eq. (14), we obtain $2q$ eigenvalues for each orbital $\phi_j(\mathbf{r})$, with $j = 1, 2, 3$. In total, this gives $6q$ eigenvalues. The eigenvalues corresponding to the valence band range from 0 to $2q$, while those of the conduction band range from $2q + 1$ to $4q$.

For instance, in Fig. 1(a), the first Landau level is labeled as $\left|0, 0\right\rangle_{K'}$. This level is degenerate, i.e., $E_{2q+1} = E_{2q+2}$, corresponding to the same energy value. Similarly, the second Landau level is labeled as $\left|0, 1\right\rangle_{K'}$, which corresponds to the two degenerate eigenvalues $E_{2q+3} = E_{2q+4}$, and so on for the subsequent Landau levels. In Fig. 1(e), for the valence band, we clearly observe the evidence of the Brillouin zone shrinking. At a given value of B, the energy value is obtained simultaneously at the K, K' and Γ points. The first Landau level in the valence band corresponds to the eigenvalue E_{2q} (labeled as $|0,0\rangle_\Gamma$), which is degenerate with E_{2q-1}. The second Landau level then corresponds to E_{2q-2} and E_{2q-3}, and so on for the lower levels.

In terms of Eq. (22), we have

$$m_e^* = \frac{eB\hbar}{E_{2q+3} - E_{2q+1}}. \tag{30}$$

However, for m_h^*, the situation is quite different and more complicated than for m_e^*. For some cases, like MoS_2, this difficulty arises because the energy of the Γ point lies close to the K and K' valleys. As a consequence, in Fig. 1(d), the eigenvalues are no longer linear or follow the sequential index $2q - n$ as in the case of m_e^*, but instead exhibit level crossings due to numerical issues. To address this, first, we need to determine the energy value E_n at a given B that corresponds to the envelope function. This can be done by plotting all the wave functions from 0 to $2q$, since each wave function provides information about the Landau level labeling. From the wave functions, we can then identify which E_n corresponds to $|j,n\rangle_\tau$.

3 Numerical results

3.1 Effective mass

Monolayer MoS_2

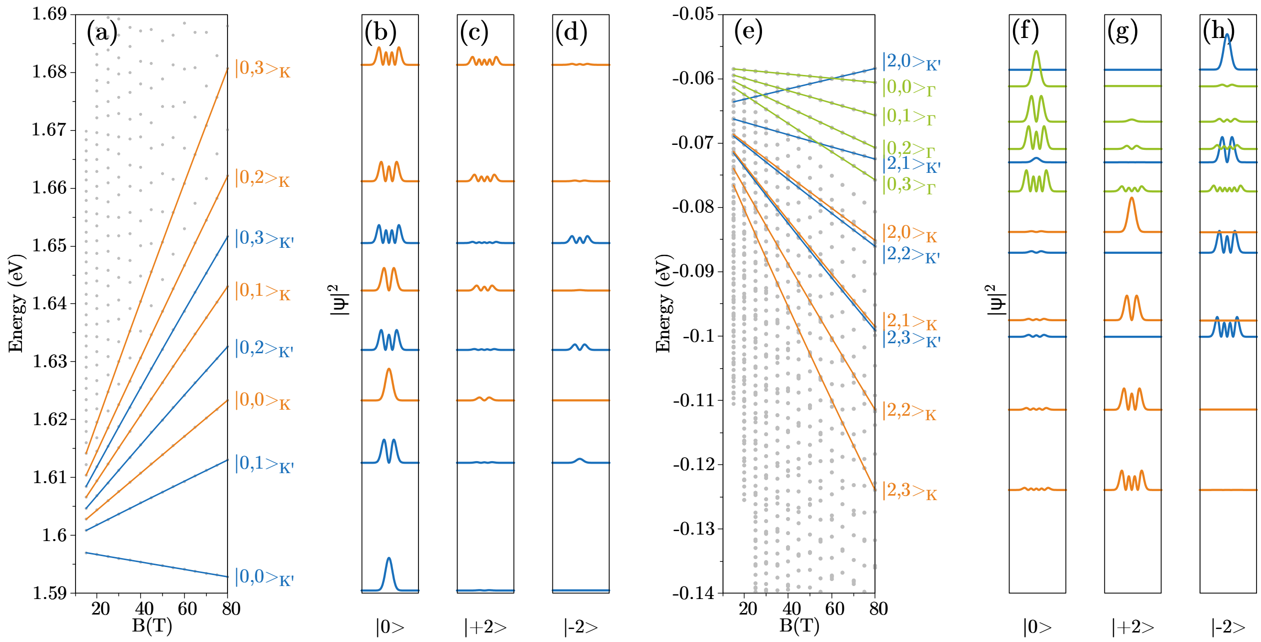

Hình 1: Landau levels (a) and the corresponding envelope-function components (b),(c),(d) for conduction electrons at valleys K and K'. Figs (e)–(h) show the same as (a)–(d) but for valence electrons. (Recalculated from Ho *et al.* [1])

The band structure of MoS_2 without a magnetic field shows that, in the valence band, the Γ point has an energy level of $E \approx -0.058$ eV. Therefore, when a magnetic field is applied, this Γ-point energy level still appears.

The effective masses of MoS_2 in the absence of a magnetic field, calculated from

$$\frac{1}{m^*_{ij}} = \frac{1}{\hbar^2}\frac{\partial^2 E(\mathbf{k})}{\partial k_i \partial k_j}, \tag{31}$$

are $m_e \approx 0.4178m_0$, $m_h \approx 0.5325m_0$, and $m_r \approx 0.2341$ for the TNN case, and $m_e \approx 0.4508m_0$, $m_h \approx 0.6487m_0$, and $m_r \approx 0.2659m_0$ for the NN case.

When a strong magnetic field is applied, for example $B = 100$ T:

a) Nearest neighbor (NN)

- At valley K: $m_h \approx 0.7011m_0$, $m_e \approx 0.4763m_0$. The reduced mass is $m_r \approx 0.2836m_0$, which increases by $\approx 6.7\%$.
- At valley K': $m_h \approx 0.6597m_0$, $m_e \approx 0.4606m_0$. The reduced mass is $m_r \approx 0.2713m_0$, which increases by $\approx 2.0\%$.

b) Third nearest neighbor (TNN)

- At valley K: $m_h \approx 0.5739m_0$, $m_e \approx 0.4573m_0$. The reduced mass is $m_r \approx 0.2545m_0$, which increases by $\approx 8.71\%$.
- At valley K': $m_h \approx 0.5584m_0$, $m_e \approx 0.4263m_0$. The reduced mass is $m_r \approx 0.2417m_0$, which increases by $\approx 3.25\%$.

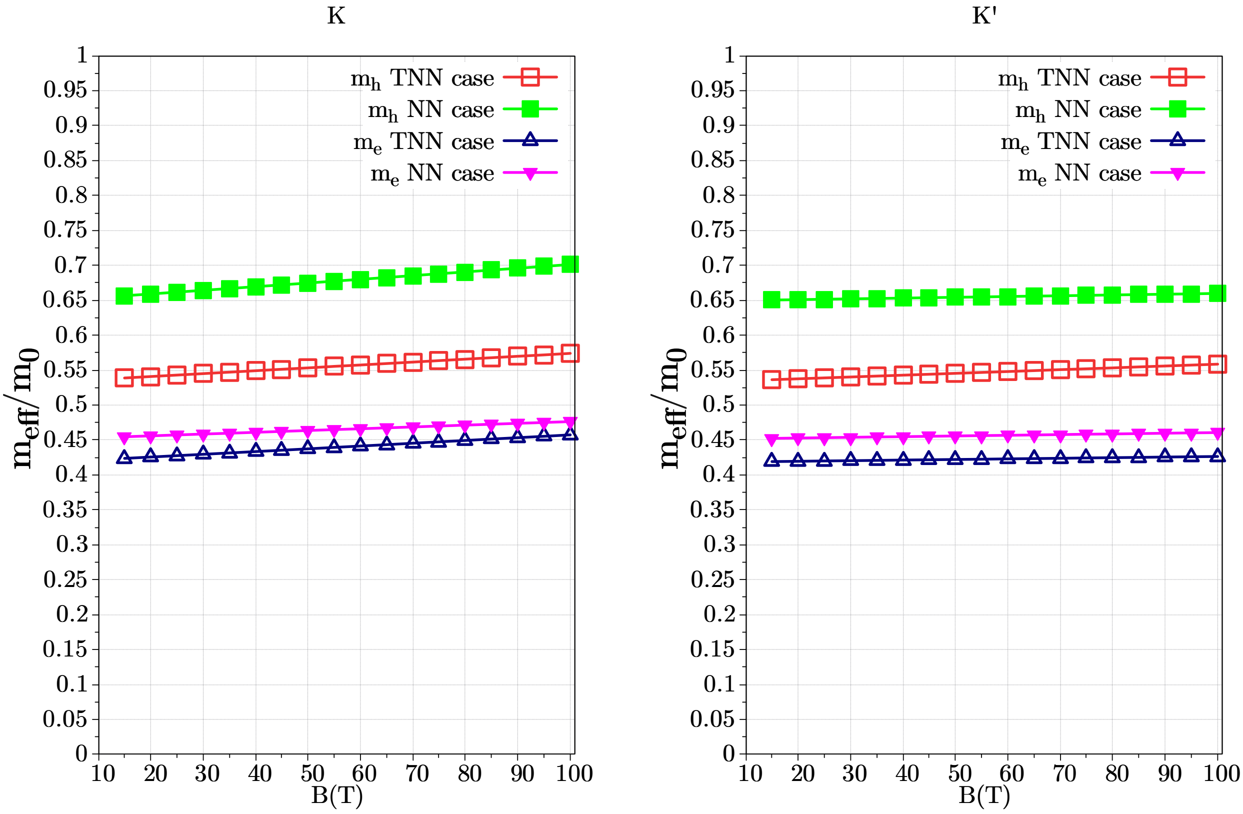

Hình 2: Effective masses.

Meanwhile, Goryca *et al.* [2] reported that $m_r \approx 0.27 \pm 0.01m_0$, which is $4\% - 10.2\%$ larger than the earlier result of Berkelbach *et al.* [3], $m_r = 0.245 \pm 0.005m_0$. Based on our calculations, we argue that the reduced mass at valley K, $m_r \approx 0.2545m_0$ with an increase of 8.71%, is consistent with the experimental findings of Goryca *et al.*.

Monolayer $MoSe_2$

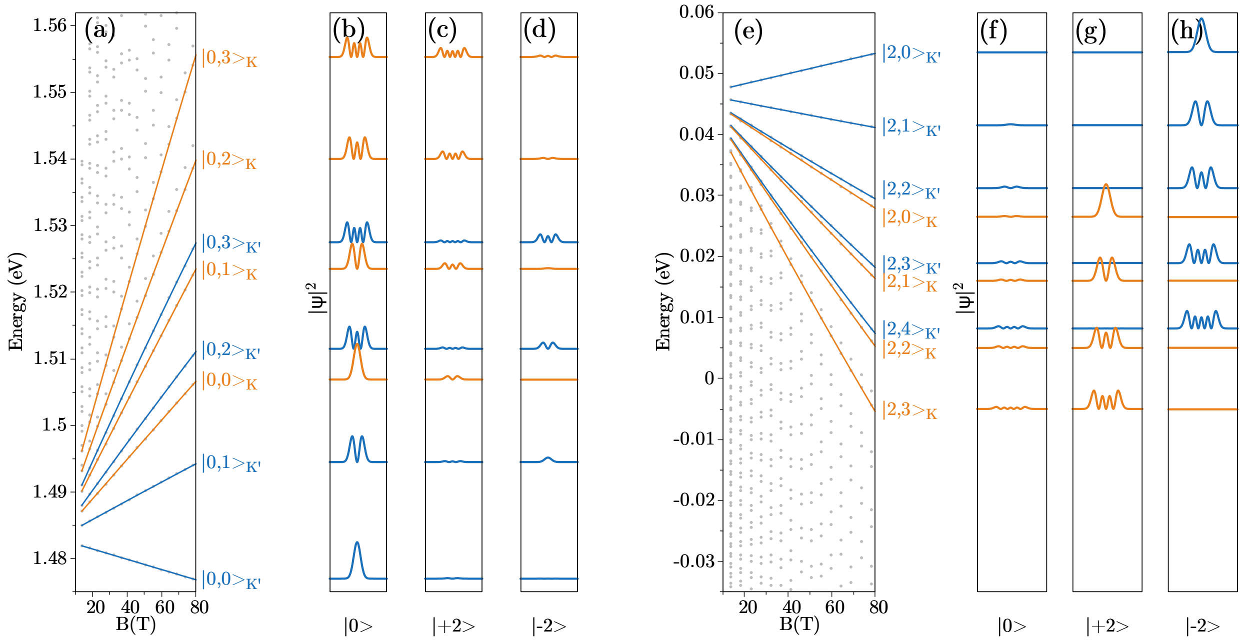

Hình 3: Landau levels (a) and the corresponding envelope-function components (b),(c) for conduction electrons at valleys K and K'. Figs (d)–(f) show the same as (a)–(c) but for valence electrons.

The band structure of $MoSe_2$ without a magnetic field shows that the Γ point does not appear near the K point. Therefore, when a magnetic field is applied, the Γ-point energy level is absent in this region. In addition, the first three Landau levels originate from the K' valley, in contrast to WSe_2, where the first two Landau levels originate from the K' valley.

The effective masses of $MoSe_2$ in the absence of a magnetic field, calculated from

$$\frac{1}{m^*_{ij}} = \frac{1}{\hbar^2}\frac{\partial^2 E(\mathbf{k})}{\partial k_i \partial k_j},$$

are $m_e \approx 0.4770m_0$, $m_h \approx 0.5887m_0$, and $m_r \approx 0.2634m_0$ for the TNN case, and $m_e \approx 0.5226m_0$, $m_h \approx 0.7512m_0$, and $m_r \approx 0.3082m_0$ for the NN case.

When a strong magnetic field is applied, for example $B = 100$ T:

a) Nearest neighbor (NN)

- At valley K: $m_h \approx 0.8100m_0$, $m_e \approx 0.5529m_0$. The reduced mass is $m_r \approx 0.3286m_0$, which increases by $\approx 6.62\%$.
- At valley K': $m_h \approx 0.7632m_0$, $m_e \approx 0.5331m_0$. The reduced mass is $m_r \approx 0.3138m_0$, which increases by $\approx 1.82\%$.

b) Third nearest neighbor (TNN)

– At valley K: $m_h \approx 0.7168m_0$, $m_e \approx 0.5320m_0$. The reduced mass is $m_r \approx 0.3052m_0$, which increases by $\approx 15.87\%$.

– At valley K': $m_h \approx 0.6251m_0$, $m_e \approx 0.4874m_0$. The reduced mass is $m_r \approx 0.2738m_0$, which increases by $\approx 3.95\%$.

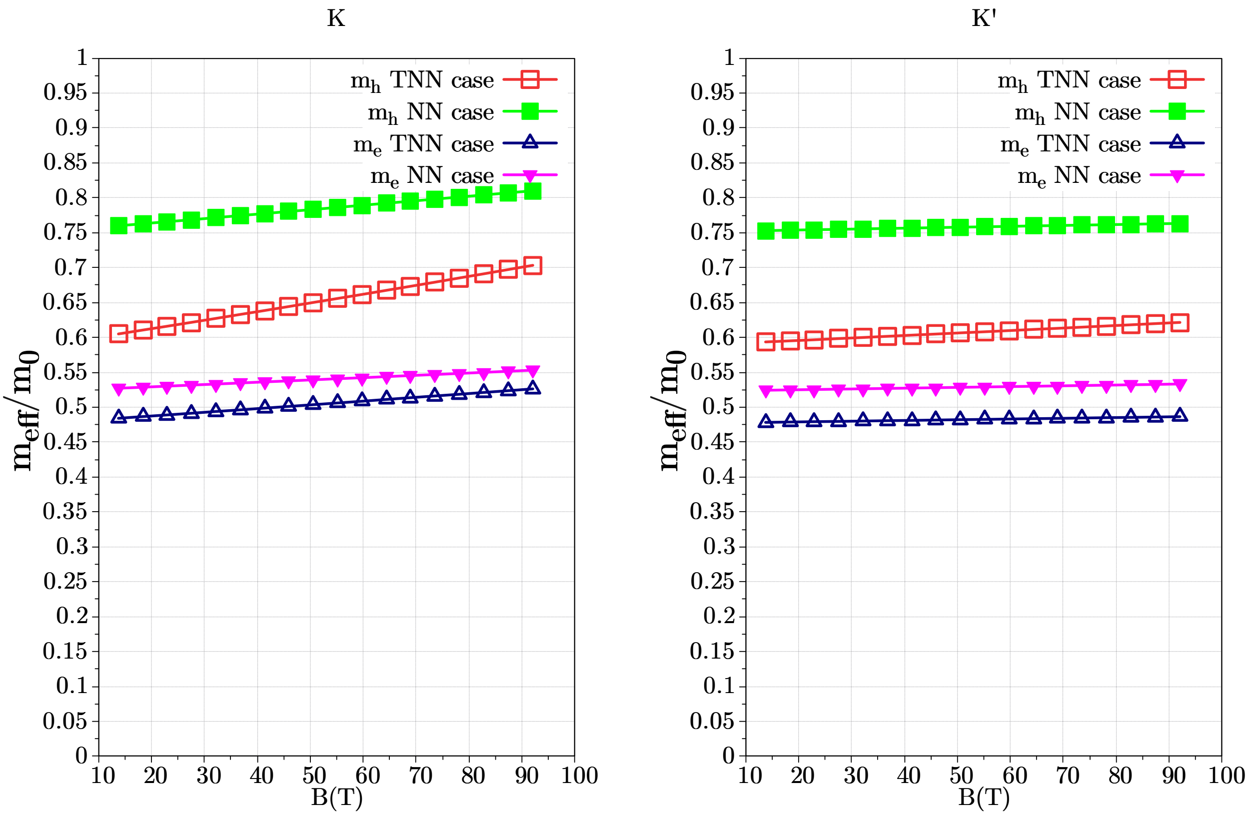

Hình 4: Effective masses.

Meanwhile, Goryca *et al.* [2] reported that $m_r \approx 0.350 \pm 0.015m_0$, which is 24.1% – 35.2% larger than the earlier result of Berkelbach *et al.* [3], $m_r = 0.27m_0$. Based on our calculations, we argue that at valley K, the reduced mass $m_r \approx 0.3052m_0$, with an increase of 15.87%, does not fully agree with the experimental findings of Goryca *et al.*.

Monolayer $MoTe_2$

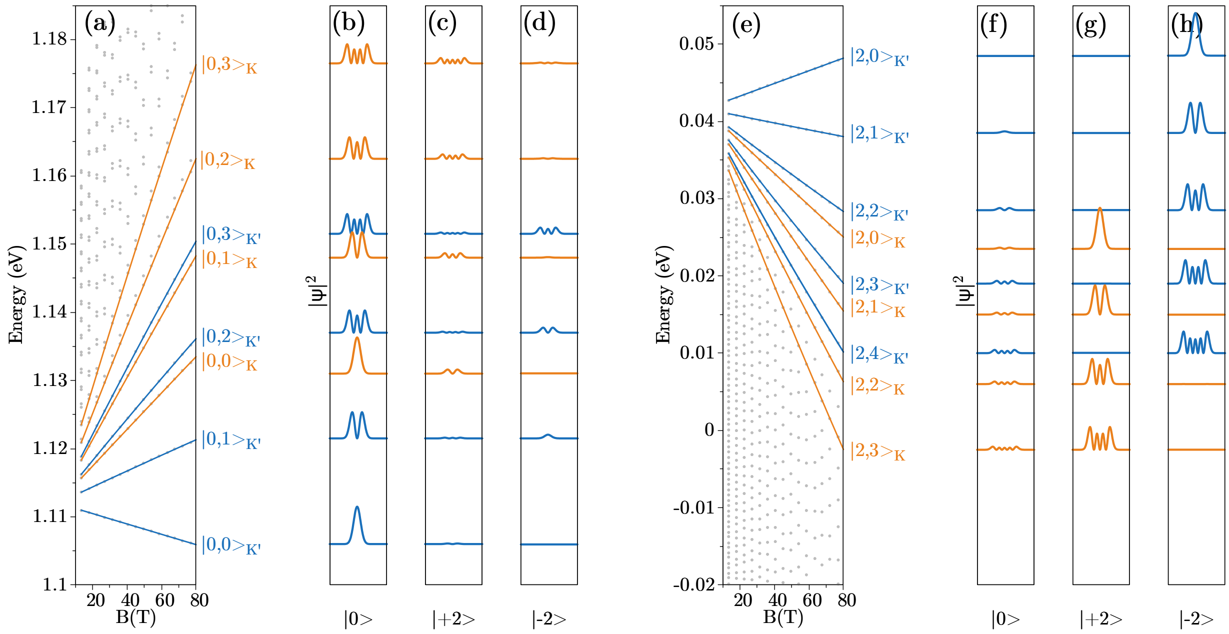

Hình 5: Landau levels (a) and the corresponding envelope-function components (b),(c) for conduction electrons at valleys K and K'. Figs (d)–(f) show the same as (a)–(c) but for valence electrons.

The band structure of $MoTe_2$ without a magnetic field shows that the Γ point has an energy level of $E \approx -0.1075$ eV. Therefore, when a magnetic field is applied, this Γ-point energy level still appears.

The effective masses of $MoTe_2$ in the absence of a magnetic field, calculated from

$$\frac{1}{m^*_{ij}} = \frac{1}{\hbar^2}\frac{\partial^2 E(\mathbf{k})}{\partial k_i \partial k_j},$$

are $m_e \approx 0.4318 m_0$, $m_h \approx 0.6044 m_0$, and $m_r \approx 0.2519 m_0$ for the TNN case, and $m_e \approx 0.5913 m_0$, $m_h \approx 0.8975 m_0$, and $m_r \approx 0.3565 m_0$ for the NN case, as also reported by Goryca *et al.* [2]. Among the six materials considered, $MoTe_2$ has the largest effective masses m_e and m_h in the absence of a magnetic field.

When a strong magnetic field is applied, for example $B = 90$ T:

a) Nearest neighbor (NN)

- At valley K: $m_h \approx 0.9774 m_0$, $m_e \approx 0.6304 m_0$. The reduced mass is $m_r \approx 0.3832 m_0$, which increases by $\approx 7.49\%$.
- At valley K': $m_h \approx 0.9142 m_0$, $m_e \approx 0.6034 m_0$. The reduced mass is $m_r \approx 0.3635 m_0$, which increases by $\approx 1.96\%$.

b) Third nearest neighbor (TNN)

– At valley K: $m_h \approx 0.7704 m_0$, $m_e \approx 0.4850 m_0$. The reduced mass is $m_r \approx 0.2976 m_0$, which increases by $\approx 18.14\%$.

– At valley K': $m_h \approx 0.6322 m_0$, $m_e \approx 0.4463 m_0$. The reduced mass is $m_r \approx 0.2616 m_0$, which increases by $\approx 3.85\%$.

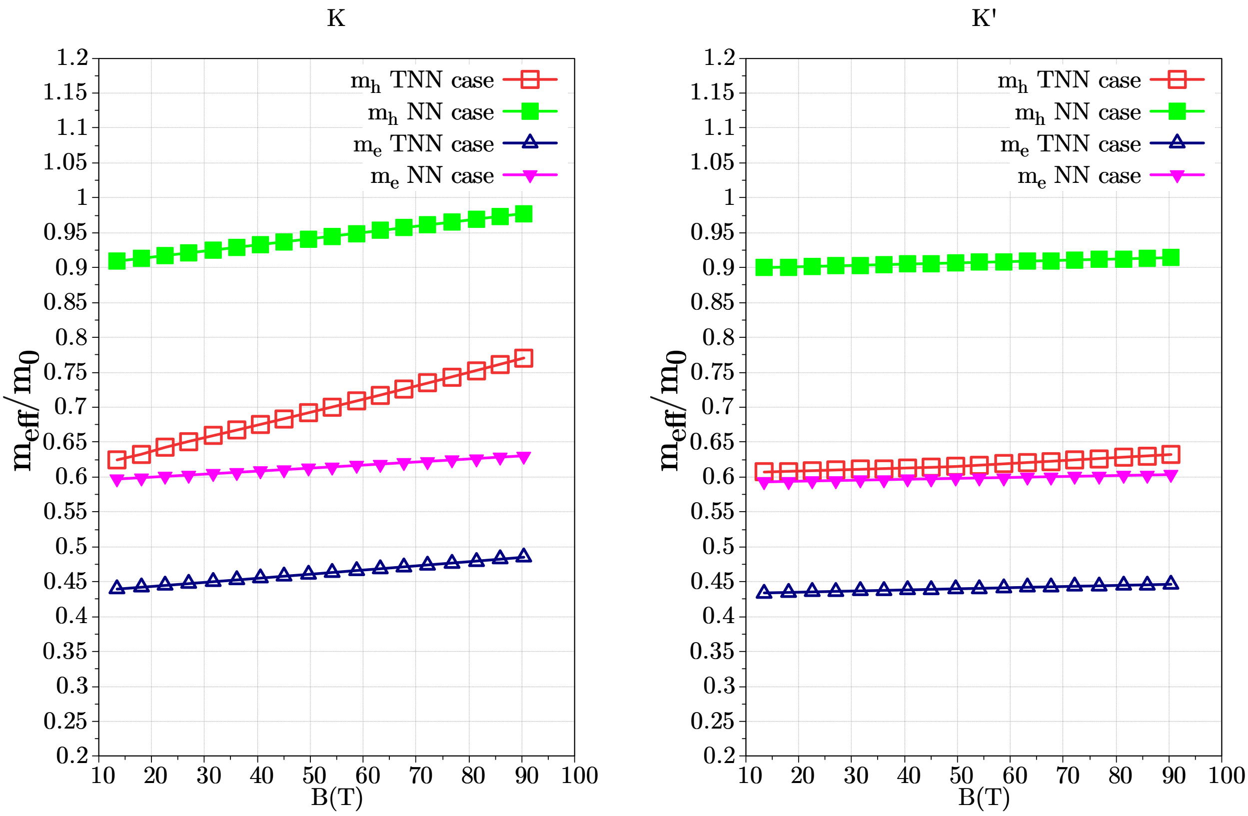

Hình 6: Effective masses.

In the study of Goryca *et al.* [2], the reduced mass was reported as $m_r = 0.36 \pm 0.04 m_0$, which is about 25% larger than the value obtained in the work of Kormányos *et al.* [4]. In our case, for the TNN model, the reduced mass is $m_r = 0.2976 m_0$, which increases by $\approx 18\%$ compared to the zero-field value $m_r = 0.2519 m_0$.

Monolayer WS_2

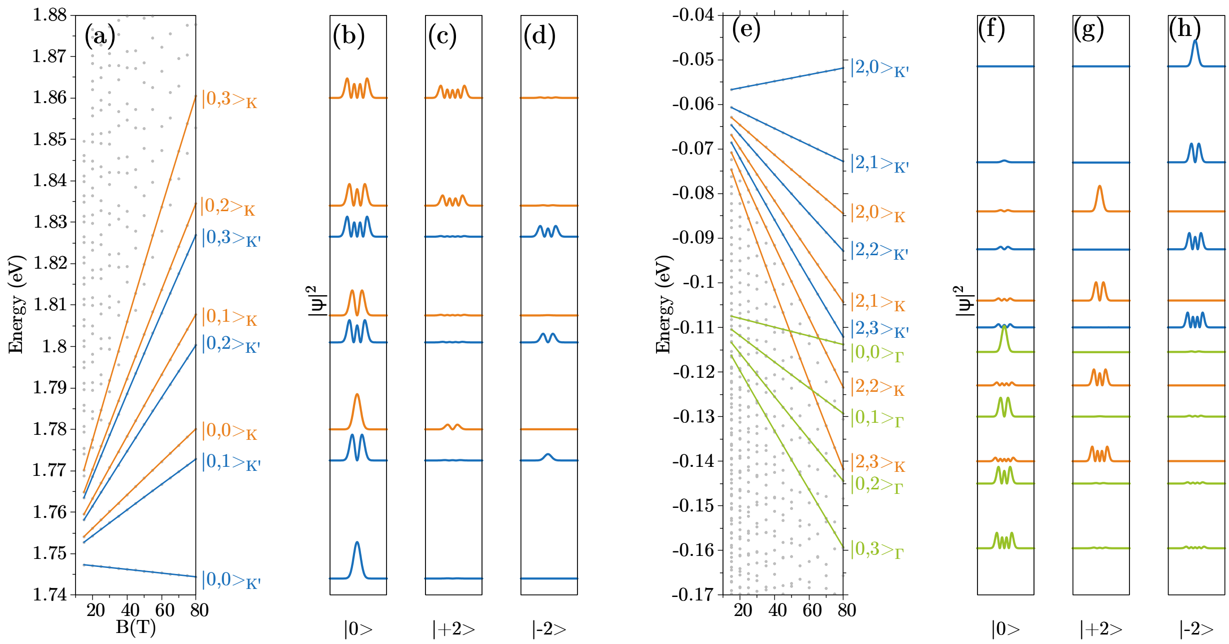

Hình 7: Landau levels (a) and the corresponding envelope-function components (b),(c) for conduction electrons at valleys K and K'. Figs (d)–(f) show the same as (a)–(c) but for valence electrons.

The band structure of WS_2 without a magnetic field shows that the Γ point has an energy level of $E \approx -0.1075$ (eV). Therefore, when a magnetic field is applied, the energy level at the Γ point still appears.

The effective mass of WS_2 without a magnetic field, calculated using

$$\frac{1}{m^*_{ij}} = \frac{1}{\hbar^2}\frac{\partial^2 E(\mathbf{k})}{\partial k_i k_j},$$

yields $m_e \approx 0.2956 m_0$, $m_h \approx 0.3845 m_0$, $m_r \approx 0.1671 m_0$ in the TNN case, and $m_e \approx 0.3195 m_0$, $m_h \approx 0.4348 m_0$, $m_r \approx 0.1841 m_0$ in the NN case.

For a strong magnetic field, e.g., $B = 100$ T:

a) Nearest neighbor

- At the K valley: $m_h \approx 0.4735 m_0$, $m_e \approx 0.3389 m_0$. Thus, $m_r \approx 0.1974 m_0$, which increases by $\approx 7.2\%$.
- At the K' valley: $m_h \approx 0.4438 m_0$, $m_e \approx 0.3273 m_0$. Thus, $m_r \approx 0.1885 m_0$, which increases by $\approx 2.3\%$.

b) Third nearest neighbor

- At the K valley: $m_h \approx 0.4205 m_0$, $m_e \approx 0.3275 m_0$. Thus, $m_r \approx 0.1841 m_0$, which increases by $\approx 10.17\%$.

– At the K' valley: $m_h \approx 0.4043m_0$, $m_e \approx 0.3023m_0$. Thus, $m_r \approx 0.1730m_0$, which increases by $\approx 3.53\%$.

In the study of Goryca *et al.* [2], they reported $m_r = 0.175 \pm 0.007m_0$, which is about 10% larger than the value $m_r = 0.15 - 0.16m_0$ obtained in the work of Berkelbach *et al.* [3].

In our case, for the K valley under the TNN approximation, we obtain $m_r \approx 0.1841m_0$ in the presence of a magnetic field, which corresponds to an increase of $\approx 10\%$ compared to $m_r \approx 0.1671m_0$ without a magnetic field. This result is consistent with and reasonable compared to the experimental findings of Goryca *et al.* [2].

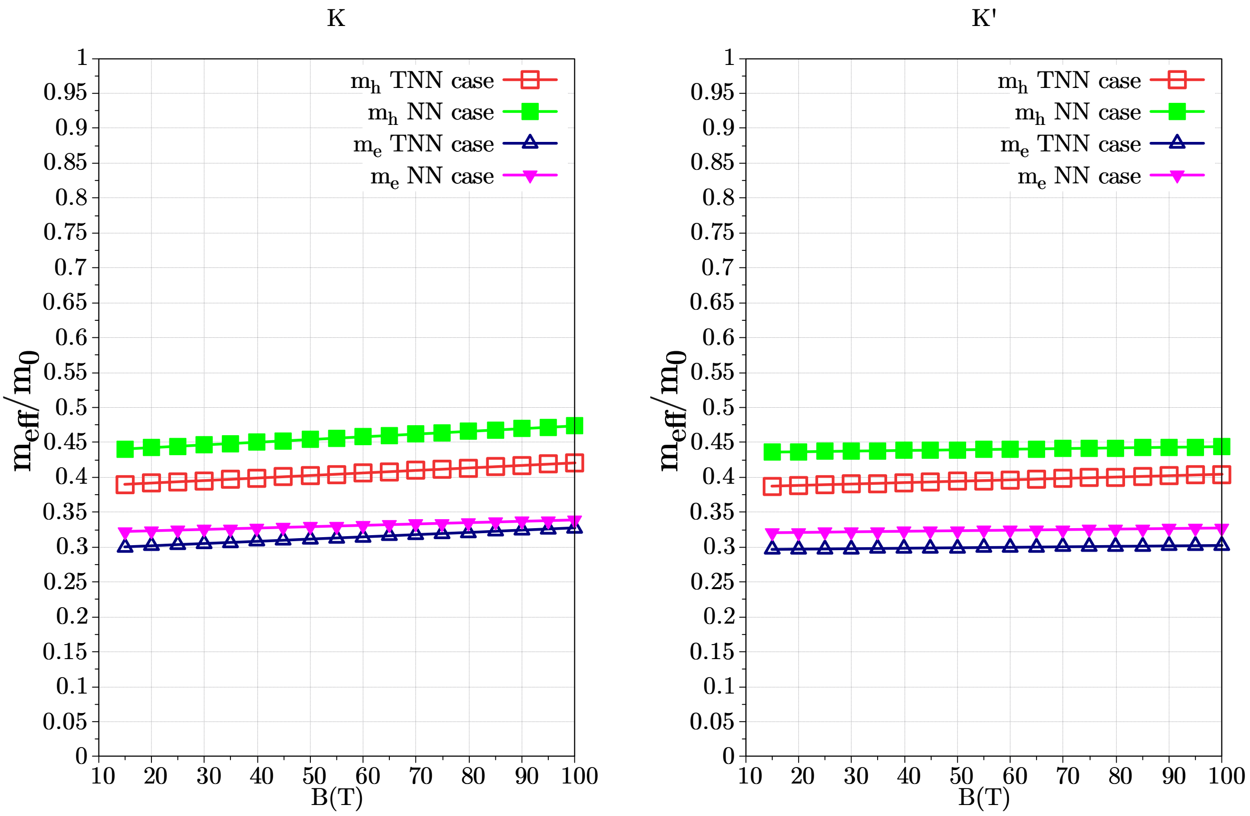

Hình 8: Khối lượng hiệu dụng.

Monolayer WSe_2

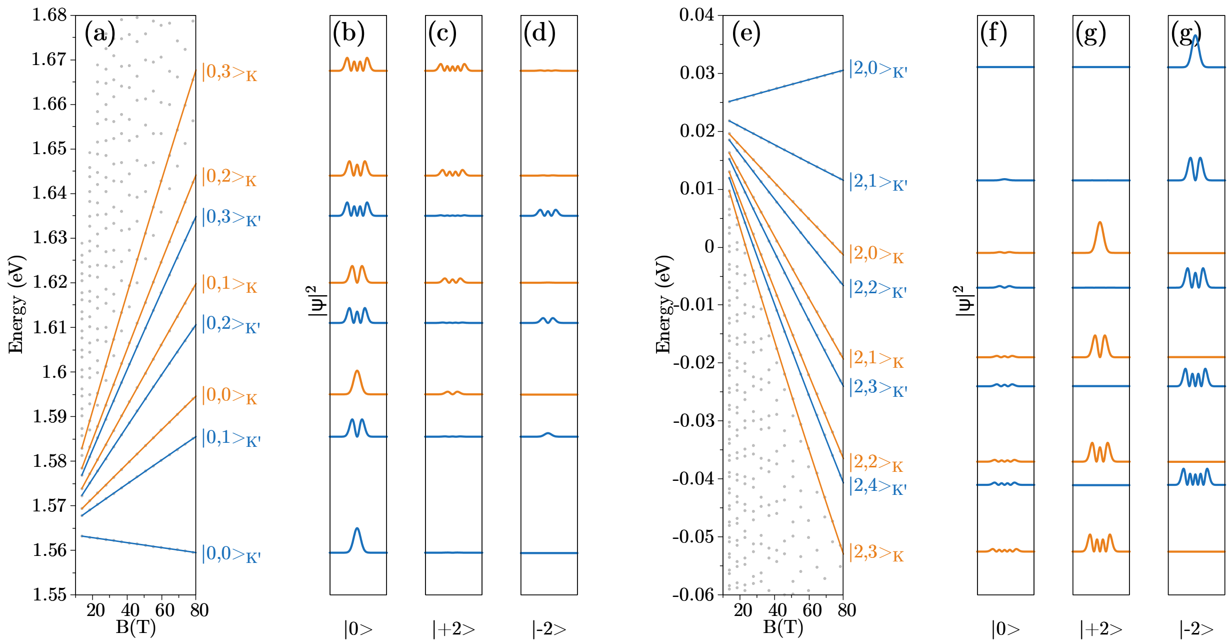

Hình 9: Landau levels (a) and the corresponding envelope-function components (b),(c) for conduction electrons at valleys K and K'. Figs (d)–(f) show the same as (a)–(c) but for valence electrons.

The band structure of WSe_2 without a magnetic field shows that the Γ point lies much lower in energy than the K point. Therefore, when a magnetic field is applied, the energy level at the Γ point does not appear here.

The effective mass of WSe_2 without a magnetic field, calculated using

$$\frac{1}{m_{ij}^*} = \frac{1}{\hbar^2}\frac{\partial^2 E(\mathbf{k})}{\partial k_i k_j},$$

yields $m_e \approx 0.3124 m_0$, $m_h \approx 0.4022 m_0$, $m_r \approx 0.1758 m_0$ in the TNN case, and $m_e \approx 0.3487 m_0$, $m_h \approx 0.4792 m_0$, $m_r \approx 0.2018 m_0$ in the NN case, as reported in the works of Kylänpää *et al.* and Berkelbach *et al.* [5, 3].

For a strong magnetic field, e.g., $B = 100$ T:

a) Nearest neighbor

- At the K valley: $m_h \approx 0.5220 m_0$, $m_e \approx 0.3702 m_0$. Thus, $m_r \approx 0.2166 m_0$, which increases by $\approx 7.34\%$.

- At the K' valley: $m_h \approx 0.4888 m_0$, $m_e \approx 0.3573 m_0$. Thus, $m_r \approx 0.2064 m_0$, which increases by $\approx 2.28\%$.

b) Third nearest neighbor

- At the K valley: $m_h \approx 0.4417 m_0$, $m_e \approx 0.3494 m_0$. Thus, $m_r \approx 0.1951 m_0$, which increases by $\approx 10.98\%$.

– At the K' valley: $m_h \approx 0.4257m_0$, $m_e \approx 0.3199m_0$. Thus, $m_r \approx 0.1826m_0$, which increases by $\approx 3.87\%$.

In the study of Stier *et al.* [6], they reported $m_r \approx 0.20 \pm 0.01m_0$, which is about 15% larger than the predictions of recent theoretical works [3, 5]. In our case, for the K valley under the TNN approximation, we obtain $m_r \approx 0.1951m_0$ in the presence of a magnetic field, corresponding to an increase of $\approx 11\%$ compared to the value without a magnetic field. This result is consistent with the findings reported by Stier *et al.* [6].

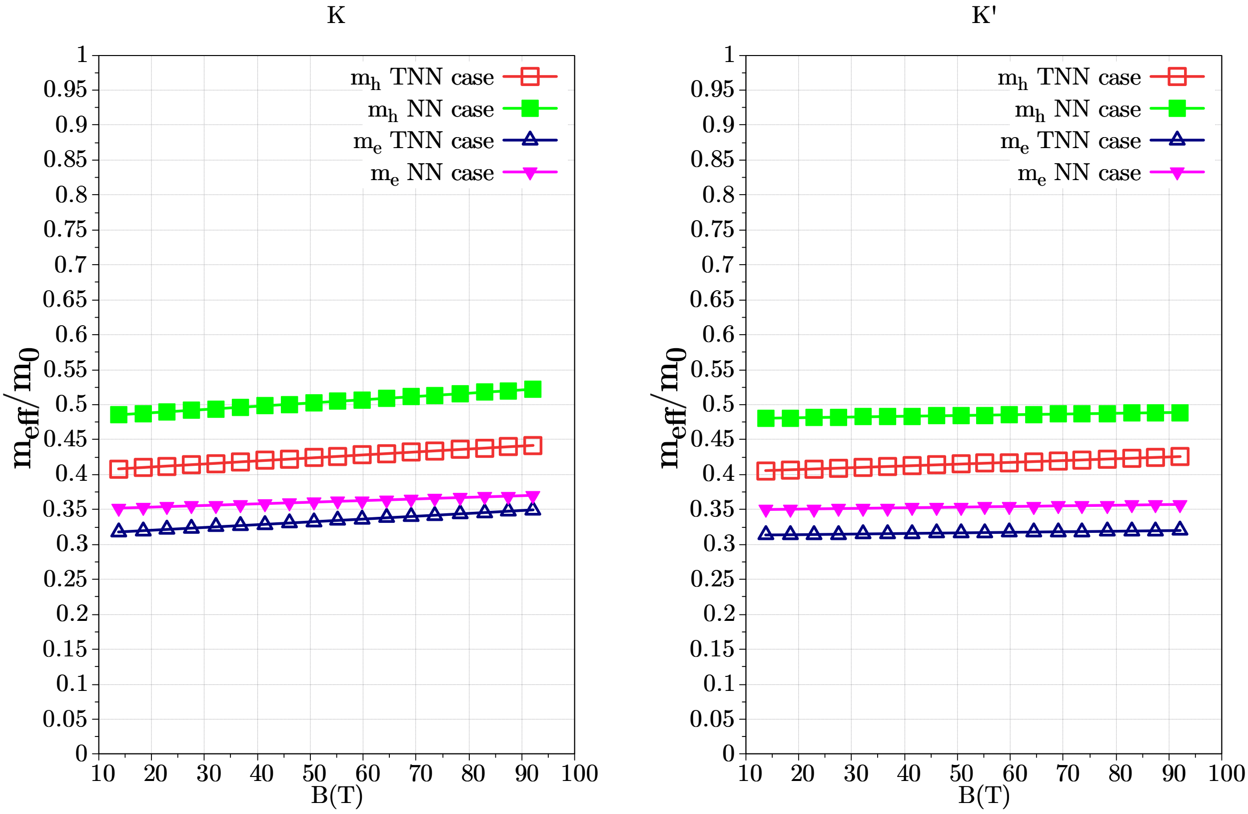

Hình 10: Khối lượng hiệu dụng.

Monolayer WTe_2

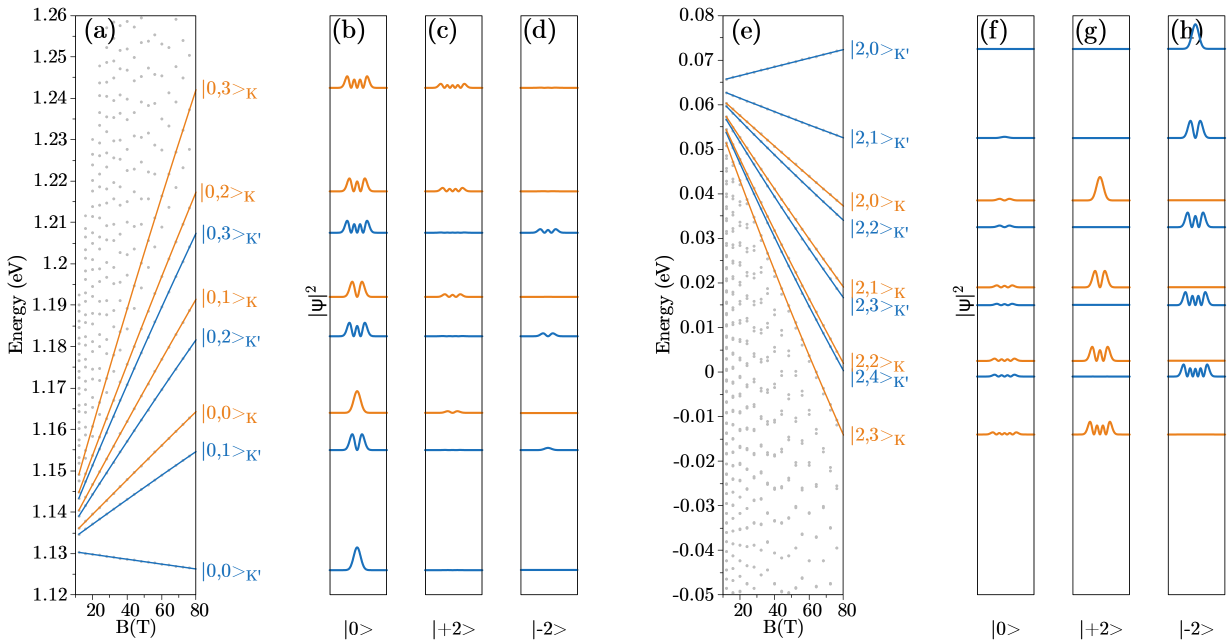

Hình 11: Landau levels (a) and the corresponding envelope-function components (b),(c) for conduction electrons at valleys K and K'. Figs (d)–(f) show the same as (a)–(c) but for valence electrons.

The band structure of WTe_2 in the absence of a magnetic field shows that the Γ point lies significantly lower in energy than the K point. Therefore, under an applied magnetic field, the Landau levels associated with the Γ point do not appear in this regime.

The effective masses of WTe_2 without a magnetic field, calculated using the formula $\frac{1}{m^*_{ij}} = \frac{1}{\hbar^2}\frac{\partial^2 E(\mathbf{k})}{\partial k_i k_j}$, are found to be $m_e \approx 0.2478 m_0$, $m_h \approx 0.3332 m_0$, and $m_r \approx 0.1421 m_0$ for the TNN case, and $m_e \approx 0.3169 m_0$, $m_h \approx 0.4559 m_0$, and $m_r \approx 0.187 m_0$ for the NN case. To the best of our knowledge, no previous studies have reported the effective masses of WTe_2.

At a high magnetic field, for example $B = 80$ T, the effective masses are obtained as follows:

a) Nearest neighbor

- At the K valley: $m_h \approx 0.5093 m_0$, $m_e \approx 0.3413 m_0$.
  This yields $m_r \approx 0.2044 m_0$, corresponding to an increase of $\approx 9.3\%$.
- At the K′ valley: $m_h \approx 0.4681 m_0$, $m_e \approx 0.3264 m_0$.
  This gives $m_r \approx 0.1923 m_0$, corresponding to an increase of $\approx 2.83\%$.

b) Third nearest neighbor

- At the K valley: $m_h \approx 0.387 m_0$, $m_e \approx 0.2824 m_0$.

This yields $m_r \approx 0.1633m_0$, corresponding to an increase of $\approx 14.92\%$.

– At the K′ valley: $m_h \approx 0.3562m_0$, $m_e \approx 0.2577m_0$.

This gives $m_r \approx 0.1495m_0$, corresponding to an increase of $\approx 5.21\%$.

Thus, at the K valley in the TNN case, the reduced mass m_r of WTe_2 exhibits an increasing of nearly 15% under a strong magnetic field, which is consistent with the trend observed for other materials discussed above.

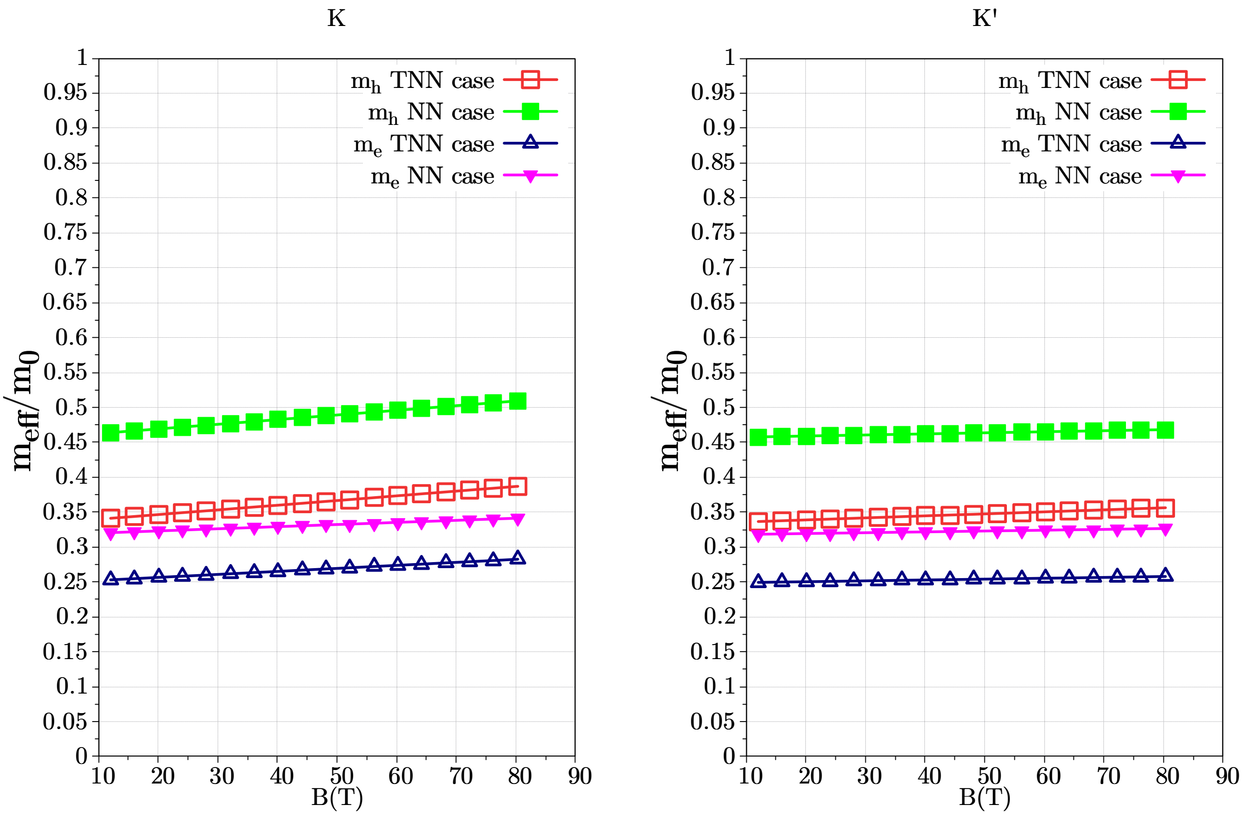

Hình 12: Khối lượng hiệu dụng.

Tài liệu

[1] Yen-Hung Ho, Yi-Hua Wang, and Hong-Yi Chen. Magnetoelectronic and optical properties of a mos 2 monolayer. *Physical Review B*, 89(15):155316, 2014.

[2] Mateusz Goryca, Jing Li, Andreas V Stier, Takashi Taniguchi, Kenji Watanabe, Emmanuel Courtade, Shivangi Shree, Cedric Robert, Bernhard Urbaszek, Xavier Marie, et al. Revealing exciton masses and dielectric properties of monolayer semiconductors with high magnetic fields. *Nature communications*, 10(1):4172, 2019.

[3] Timothy C Berkelbach, Mark S Hybertsen, and David R Reichman. Theory of neutral and charged excitons in monolayer transition metal dichalcogenides. *Physical Review B—Condensed Matter and Materials Physics*, 88(4):045318, 2013.

[4] Andor Kormányos, Guido Burkard, Martin Gmitra, Jaroslav Fabian, Viktor Zólyomi, Neil D Drummond, and Vladimir Fal'ko. k· p theory for two-dimensional transition metal dichalcogenide semiconductors. *2D Materials*, 2(2):022001, 2015.

[5] Ilkka Kylänpää and Hannu-Pekka Komsa. Binding energies of exciton complexes in transition metal dichalcogenide monolayers and effect of dielectric environment. *Physical Review B*, 92(20):205418, 2015.

[6] Andreas V Stier, Nathan P Wilson, Kirill A Velizhanin, Junichiro Kono, Xiaodong Xu, and Scott A Crooker. Magnetooptics of exciton rydberg states in a monolayer semiconductor. *Physical review letters*, 120(5):057405, 2018.